Adsorbate Screening of Surface Charge of Microscopic Ferroelectric Domains in Sol–Gel PbZr_0.2 Ti_0.8 O_3 Thin Films

O. Copie, Nicolas Chevalier, Gwenael Le Rhun, Cindy Lynn Rountree, Dominique Martinotti, Sara Gonzalez, Claire Mathieu, Olivier Renault, Nicholas Barrett

Adsorbate Screening of Surface Charge of Microscopic Ferroelectric Domains in Sol−Gel PbZr$_{0.2}$Ti$_{0.8}$O$_3$ Thin Films

Olivier Copie,[†,∥] Nicolas Chevalier,[‡,§] Gwenael Le Rhun,[‡,§] Cindy L. Rountree,[†] Dominique Martinotti,[†] Sara Gonzalez,[†] Claire Mathieu,[†] Olivier Renault,[‡,§] and Nicholas Barrett*,[†]

[†]SPEC, CEA, CNRS, Université Paris-Saclay, CEA Saclay, 91191 Gif-sur-Yvette Cedex, France
[‡]Univ. Grenoble Alpes, 38000 Grenoble, France
[§]CEA, LETI, MINATEC Campus, 38054 Grenoble, France
[∥]Institut Jean Lamour, UMR 7198 CNRS/Université de Lorraine, 54056 Vandœuvre-lès-Nancy, France

ABSTRACT: We present a study of adsorbate screening of surface charge in microscopic ferroelectric domains in a sol−gel grown PbZr$_{0.2}$Ti$_{0.8}$O$_3$ thin film. Low-energy and photoemission electron microscopies were employed to characterize the temperature dependence of surface charge and polarization of ferroelectric domains written by atomic force microscopy. We study the role of charged adsorbates in screening of polarization-bound charges. We demonstrate that full-field electron microscopy is suitable for the determination of ferroelectric system properties such as the Curie temperature.

KEYWORDS: PZT, polarization, screening, surface, LEEM, PEEM, PFM, AFM
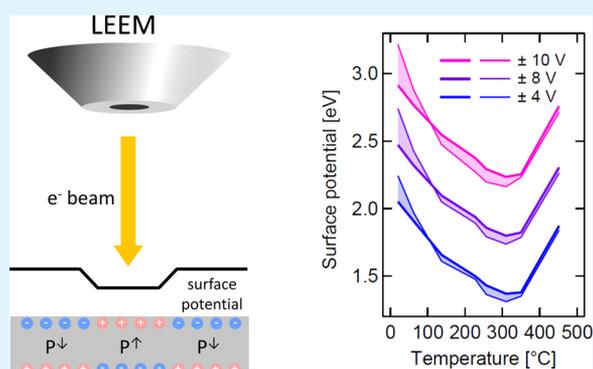
1. INTRODUCTION

Ferroelectric (FE) materials are characterized by the development of a spontaneous electric polarization below a critical temperature T_C, the Curie temperature. At the surface, polarization **P** induces a surface charge, $\sigma = \mathbf{P} \cdot \mathbf{n}$ (**n**, unit vector normal to the surface), in turn creating a depolarizing field, E_{dep}, which can be detrimental to the FE stability of very thin films.[1] To sustain the FE state, E_{dep} must be at least partially compensated, for example, by screening of the surface charge. In turn, this may modify the surface chemistry. Control of the polarization can tailor domain-specific surface reactivity and potentially paves the way toward the design of nanoscale chemical devices.[2] Understanding screening is therefore a key issue in view of a wide range of applications.

The charge compensation mechanisms may be related to bulk defects, such as oxygen vacancies and/or extrinsic absorbate species like water. There has been an increasing interest in considering FE surfaces for chemical reactions and catalytic applications.[3] Polarization-orientation-dependent adsorption of metal and carbon dioxide onto BaTiO$_3$ or PbZr$_{0.48}$Ti$_{0.52}$O$_3$ and 2-propanol molecules onto LiNbO$_3$ have been demonstrated recently.[4,5] The role of water is crucial at the FE surface: (i) it promotes the mobility and diffusion of the adsorbed species and (ii) it can be adsorbed through molecular (H$_2$O) or dissociative (HO$^-$ and H$^+$) bonding to the surface.[6] Charge transfer subsequent to HO$^-$ and H$^+$ adsorption onto PbTiO$_3$ can stabilize upward and downward pointing polarizations, respectively.[7] Screening by polar adsorbates can lead to

surface potential inversion, as measured by electrostatic and Kelvin probe force microscopy,[8−10] whereas polarization switching can be rapid; the relaxation of the surface screening charge may be much slower.[8] The slow relaxation of the screening charge may also determine the domain wall movement.

Although efficient, lead-free ferroelectric and piezoelectric materials have been proposed;[11] the best properties are still exhibited by lead-based compounds, such as Pb(Zr,Ti)O$_3$ (PZT).[12,13] The piezoelectric properties are strongly enhanced at the morphotropic phase boundary,[14] making PbZr$_{0.52}$Ti$_{0.48}$O$_3$ films suitable for many applications, for example, microelectromechanical systems.[15] On the other hand, the FE response is maximum for Ti-rich PZT, making such films more suitable for applications in electronics.

Many model thin-film systems are realized using molecular beam epitaxy or pulsed laser deposition,[16] and enhanced properties could be obtained, for example, $T_C \approx 680$ °C in sputtered epitaxial PbZr$_{0.2}$Ti$_{0.8}$O$_3$ thin film.[17] However, these growth techniques require high or ultrahigh vacuum, are expensive, and cannot process large-area substrates. They are therefore far from being industry viable. Metal-organic chemical vapor-deposited Ti-rich PZT films between 50 nm and 1.2 μm thick showed high polarization values between 30 and 55 μC/

cm^2.[18] Soft chemistry methods such as sol–gel growth[19,20] could be a practical alternative with good film homogeneity on industrial-scale substrates[12] but only if FE properties similar to those obtained by, for example, pulsed laser-deposited layers were to be observed. Sol–gel growth of PZT on Si substrates is well established.[19,21,22] An earlier work reports on thicker films,[21] whereas more recent work uses SrTiO$_3$-buffered Si yielding high-quality 70 nm PZT films.[22] Atomic force microscopy (AFM) studies have focused on poling by application of a potential difference between the tip and the bottom electrode and characterization of the piezoresponse of the PZT layer.[21] Much less attention has been devoted to study of the surface charge. Nevertheless, surface water is omnipresent under atmospheric conditions and works as a thin conducting layer or electrode, determining domain growth under an applied electric field.[23] Therefore, the characterization of such films requires accurate measurement of the Curie temperature, FE stability, as well as the charge screening mechanisms and surface chemistry.

Experiments in vacuum are beneficial to some extent in avoiding uncontrolled adsorbate screening. Electrons are sensitive to both polarization and screening charge. Le Bihan developed the use of secondary electron emission in a scanning electron microscope to probe the surface charge in BaTiO$_3$.[24] Ihlefeld et al. have used backscattered electrons to image FE domains in thin films.[25] However, sample charging is a recurrent problem when using electron beams with higher primary energy. Low-energy electron microscopy (LEEM), on the other hand, is particularly suited to probe the surface potential.[26] In fact, at very low energy, incident electrons are reflected by the surface potential; this is called mirror electron microscopy (MEM). As a result, they only interact weakly with the sample and allow accurate mapping of the surface potential while avoiding charging effects usually associated with insulating samples. At higher energy they penetrate the sample and are backscattered (LEEM). The MEM–LEEM transition provides a direct map of the surface potential.

In photoemission electron microscopy (PEEM), imaging threshold intensity as a function of kinetic energy allows the photoemission threshold to be mapped.[26,27] PEEM can also be used in absorption mode to study the domain orientations and surface charge.[28]

The surface potential may also be measured using near-field microscopy techniques. In particular, electrostatic force microscopy (EFM) is sensitive to the force gradient between surface and tip and Kelvin force microscopy (KFM), also known as scanning surface potential microscopy, measures the force.[8] In both cases, the technique requires scanning and careful consideration of the tip–surface interactions. For example, the potential measured by KFM depends directly on the tip–surface distance. LEEM, on the other hand is a full-field, noncontact technique, which may allow faster acquisition without potential tip–surface perturbations, although LEEM techniques require an ultrahigh vacuum sample environment and precise alignment of the electron optics system.[26]

In Figure 1, we represent schematically the expected photoelectron (black arrow) and reflected electron (dashed arrow) interaction with a charged FE surface, in this case, a surface screened by polar adsorbates. The FE film is out-of-plane polarized; we denote the polarization pointing away from the substrate to the surface as P$^+$ and the polarization pointing toward the substrate as P$^-$. The adsorbate layer induces an electric field **E**$_S$ in the near-surface region. Photoemitted
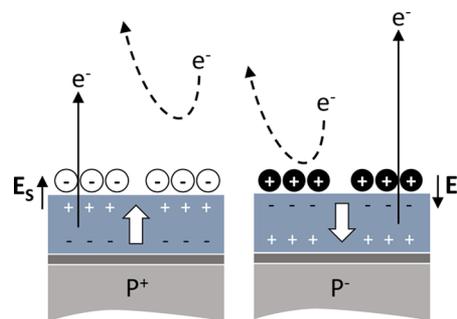

Figure 1. Screening of P$^+$ (P$^-$) polarization by negatively (positively) charged adsorbates induces an electric field (**E**$_S$) in the very near-surface region. Photoemitted (PEEM) electrons are represented by straight black arrows. Incident (LEEM) electrons are represented by black dashed lines.

electrons are slowed down and accelerated for P$^+$ and P$^-$ domains, respectively. The photoemission threshold of P$^+$ domains is higher than that of P$^-$ domains. Local differences in threshold can be used to estimate both the surface charge and polarization.[29] Incident electrons see negative and positive surface potential for screened P$^+$ and P$^-$ domains, respectively. The MEM–LEEM transition is at a higher incident energy for screened P$^+$ than for screened P$^-$ domains and lower incident energy for unscreened P$^+$ than for P$^-$ because the positive surface charge attracts the incident electrons into the sample. The reduction of the surface potential contrast between oppositely polarized domains in BaTiO$_3$ by screening charge has been demonstrated using LEEM.[30]

Here, we report on the study of the surface of a sol–gel PbZr$_{0.2}$Ti$_{0.8}$O$_3$ FE thin film. After initial characterization by PEEM of AFM-written domains, LEEM was employed to measure the temperature dependence of the surface potential contrast and the adsorbate-induced changes in the surface charge. The Curie temperature of the sol–gel film is ∼430 °C. The contrast observed in both PEEM and LEEM is directly correlated with the phase signal in piezoresponse force microscopy (PFM) and the surface potential as measured by KFM and hence the domain polarization. The samples used in both PEEM and LEEM studies had been exposed to air prior to introduction into the UHV systems. The relative contrast in the LEEM images is clear evidence of adsorbate screening of the surface polarization charge at room temperature and desorption at higher temperature.

2. EXPERIMENTAL SECTION

PbZr$_{0.2}$Ti$_{0.8}$O$_3$ (PZT) thin films (56 nm thick) were deposited on the Pt(100 nm)/TiO$_2$(20 nm)/SiO$_2$(500 nm)/Si substrate by the sol–gel method.[19] A Si wafer is chosen so that the process is as compatible as possible with the current semiconductor technology. The PbZr$_{0.2}$Ti$_{0.8}$O$_3$ stoichiometry was chosen to maximize the FE response of the material.[31] SiO$_2$ is a thermal oxide grown at 1100 °C in oxygen for passivation. TiO$_2$ was obtained by sputter-depositing 10 nm of Ti followed by thermal annealing at 700 °C in oxygen for 30 min. TiO$_2$ is needed to ensure a good adhesion for platinum (Pt) bottom electrode and for preventing the lead diffusion from PZT during film growth. The Pt bottom electrode was sputtered at 450 °C. PZT solution, provided by Mitsubishi Materials Corporation, is spin-coated on the 200 mm preprocessed, platinized Si substrate. The typical spin-coating parameters are 1000 rpm for rotation speed, 1500 rpm/s for acceleration, and 20 s for the spin duration. After the coating step, the wafer is dried on a hot plate at 130 °C for 5 min so as to evaporate the solvents. Calcination (or pyrolysis) is then done at 360 °C for 5
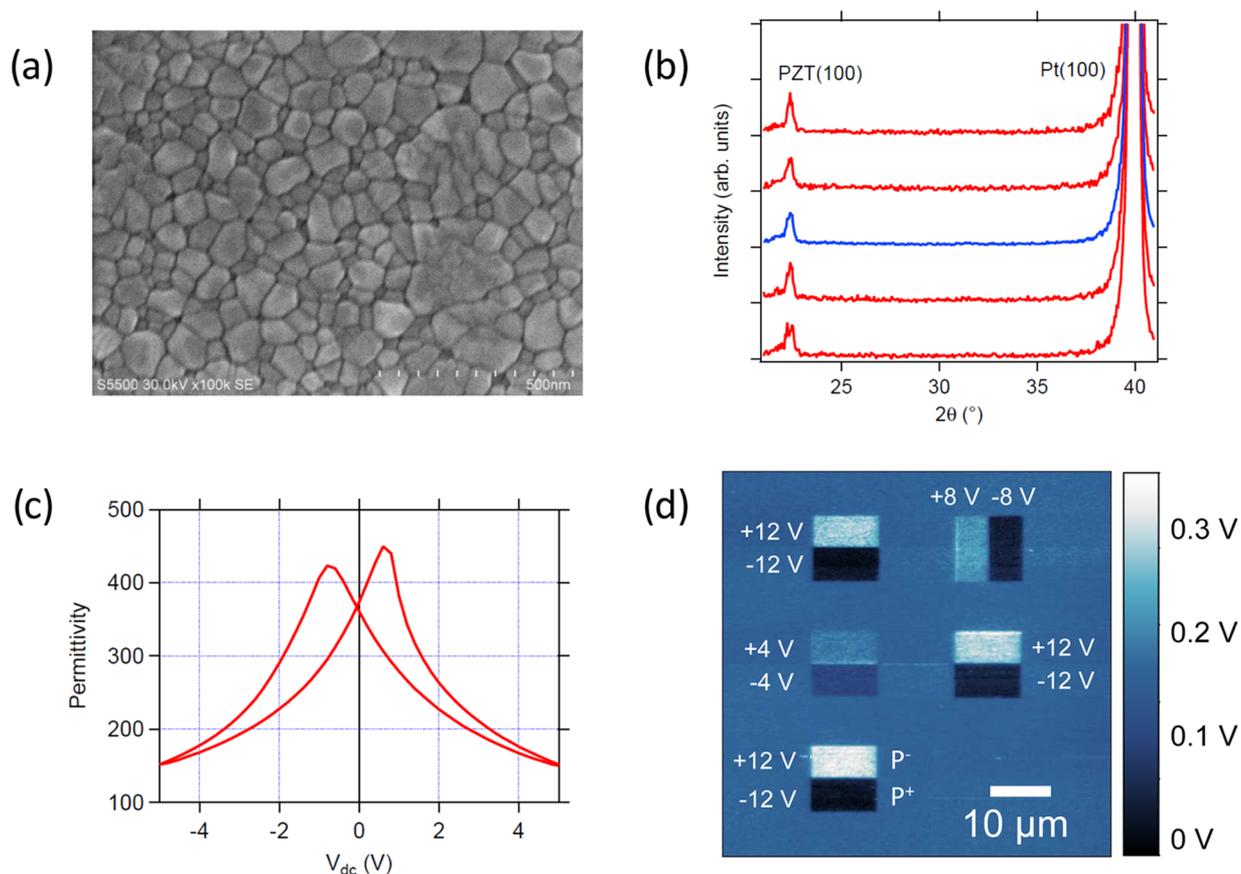
Figure 2. (a) Scanning electron microscopy image using backscattered electrons of the PZT surface. (b) X-ray diffraction $\theta-2\theta$ scans (red lines) at four different points on the 200 mm wafer showing a highly textured, (100)-oriented film. The middle (blue) curve is the average of the four scans. (c) $C-V$ characteristics carried out at 100 kHz showing an almost perfectly symmetrical butterfly loop, characteristic of a good ferroelectric (d) Surface potential (V) image of the microscopic written FE domains, as measured by KFM. Each domain is $5 \times 10 \ \mu m^2$ and is either outward or inward polarized (P^+ and P^-, respectively).

min to eliminate organic compounds. Finally, the crystallization of the amorphous PZT film is performed in a rapid thermal annealing furnace, where PZT is heated at 700 °C for 1 min in pure oxygen flux.

The microstructure probed by SEM shown in Figure 2a did not show any evidence of parasitic surface phases. A large, compact grain structure is evident without any evidence for the distinct surface phase often present in sol−gel PZT,[20] with stoichiometry near the morphotrophic phase boundary. The crystalline phase was investigated by X-ray diffraction. Figure 2b shows $\theta-2\theta$ scans (red lines) at four different points on the 200 mm wafer. At all points, a clear (100)-oriented growth with a tetragonal structure, with an in-plane lattice parameter of 3.97 Å, is observed. The $C-V$ characteristic at 100 kHz shown in Figure 2c has an almost perfectly symmetrical butterfly loop, attesting to the strong FE response of the 56 nm film. The patterning of microsized FE domains for PEEM analysis was performed by AFM (Bruker Dimension Icon with Nanoscope V electronics) in contact mode under N_2 atmosphere (performed in a nitrogen-filled glove box (MBraun), with H_2O and O_2 contents below 3 ppm). We used a standard PtIr-coated silicon cantilever (SCM-PIT from Bruker) with a nominal spring constant of 2.8 N/m. The applied force was maintained below 100 nN to avoid mechanical damage of the PZT layer. The direct current (DC) voltage (V) was applied to the tip, whereas the bottom electrode was grounded. The domains for the LEEM experiment were written on a sample cut from the same wafer using an AFM (Bruker Dimension Icon with Nanoscope V electronics) under ambient conditions using the same type of tip (SCM-PIT). The domain reading was then performed using the same setup in PFM or KFM mode. In PFM, an alternating current (AC) voltage with amplitude of 1 V and a modulation close to the contact resonant frequency (330−370 kHz) was applied between the tip and

the bottom electrode. The cantilever vibration was detected using a conventional lock-in technique. The relative surface potentials were acquired by standard KFM in double pass (under N_2 atmosphere). The KFM results are shown in Figure 2d and are discussed below in introduction to the PEEM and LEEM results. In the first pass, the topography was measured in tapping mode, whereas in the second pass, the relative surface potential was measured in amplitude modulation mode at a lift height of 20 nm. The cantilever is electrically excited by an AC modulation voltage with amplitude of 2.5 V and a frequency of 68 kHz. All AFM measurements were performed in a nitrogen-filled glove box (MBraun) with H_2O and O_2 contents below 3 ppm.

Energy-filtered PEEM experiments were carried out using a NanoESCA instrument (ScientaOmicron) and Hg lamp (emission centered at 4.9 eV) as the excitation source. The pass energy setting of 50 eV and 1.0 mm analyzer slit gave an overall energy resolution of 200 meV. The photoemission threshold image series was acquired from $E-E_F$ = 4.2 to 6.5 eV in 0.025 eV steps. The exposure time per image was 6 s. PEEM measurements were performed at room temperature.

LEEM experiments were performed using a LEEM III microscope (Elmitec GmbH). The incident electron beam was emitted by a thermionic LaB_6 electron gun with a bandwidth of 0.5 eV and at an accelerating voltage of −20 kV. Low electron beam currents (20 nA) were used to make any possible charging problems under the beam negligible. The MEM−LEEM image series were acquired for electron kinetic energy with respect to the sample (also called the start voltage) from 0 to 6 eV in 0.05 eV steps.

The electron images are presented using a gray intensity scale, whereas surface potential maps are presented using a false color scale.
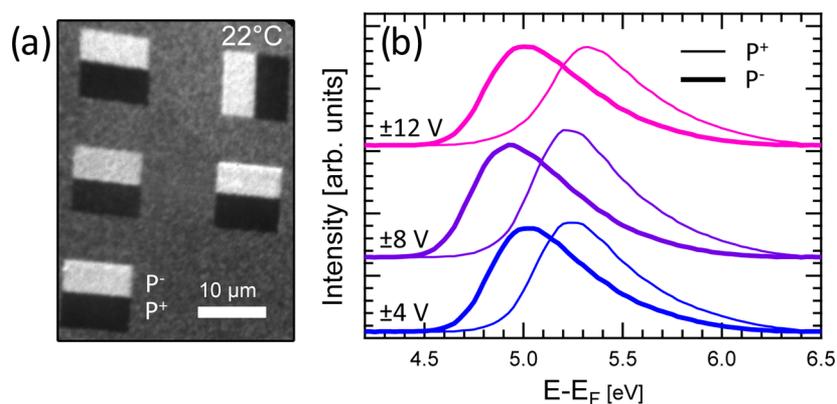
Figure 3. (a) PEEM image at $E-E_F$ = 4.9 eV recorded at 22 °C. (b) Threshold spectra extracted from the P$^+$ and P$^-$ domains written with different DC voltage amplitudes.

Complementary XPS measurements were performed using a nonmonochromtic Al Kα X-ray source and a 7 channeltron EA125 hemispherical analyzer (both ScientaOmicron). Pass energy of 20 eV and energy steps of 0.1 eV were used. The entrance and exit slits were set to 6 × 12 and 5 × 11 mm^2, respectively.

3. RESULTS AND DISCUSSION

The patterning of microscopic FE domains was performed by applying a DC voltage to the AFM tip with the bottom electrode grounded. In this way 5 × 10 μm^2 domains were written using ±12, ±10, ±8, and ±4 V. Figure 2d presents the KFM image of the surface potential of a written PZT film at room temperature. A negatively biased AFM tip induces a positive surface charge corresponding to a P$^+$ state (upward oriented polarization), whereas a positively biased AFM tip induces a negative surface charge that corresponds to a P$^-$ state (downward oriented polarization). The surface charge modifies the electrostatic surface potential measured by KFM. The potential differences between P$^+$ and P$^-$ are 0.05, 0.20, and 0.30 V for the domains written at ±4, ±8, and ±12 V, respectively.

In Figure 3a, we present a PEEM image, recorded at 22 °C, and $E-E_F$ = 4.9 eV, where E_F is the sample-holder Fermi level of the AFM-written P$^+$ and P$^-$ domains. The contrast between the oppositely polarized domains reproduces the pattern detected by KFM (Figure 2d). The image series was recorded to extract the photoemission threshold spectra from the P$^+$ and P$^-$ domains before annealing. The spectra, integrated over a single domain in each case, are shown in Figure 3b. By fitting the threshold spectra using an error function, we determined the shift in threshold between FE poled domains to be 0.24, 0.33, and 0.49 eV for 4, 8, and 12 V poling voltages, respectively. The KFM and PEEM results are reported in Table 1.

After annealing at 547 °C under UHV conditions, we can see in the PEEM image of Figure 4a that the FE domains have disappeared. This is consistent with the crossing of the ferroelectric−paraelectric transition, whose bulk Curie temperature is T_C = 430 °C,[13] and the loss of any FE memory of the domain structure. Following the high temperature annealing, new FE domains could still be written, as shown in the PFM phase image of Figure 4b, indicating that the disappearance of PEEM contrast observed in Figure 4a was not due to film decomposition but indeed due to the loss of FE memory above the FE−PE phase transition. This is supported by X-ray photoemission spectroscopy (XPS) performed on the film before and after the annealing process, shown in Figure 4c. The spectra are very similar and show no evidence of features typical of the presence of new chemical phases, for example, the phase separation of Zr oxide,[20] or significant oxygen vacancy concentration.

In Figure 5a, we show a PFM phase image of domains written at ±4, ±8, and ±10 V for the LEEM experiments. Figure 5b displays a schematic of the patterned domains. In Figure 5c, we present a LEEM image of the same domains with an incident electron kinetic energy E_{inc} = 2.30 eV, acquired at room temperature. We observe that the contrast reproduces the PFM image in Figure 4a. The granularity of the electron images corresponds to the highly textured PZT microstructure revealed in Figure 2a,b. By varying the incident energy from 0 to 6 V, we recorded a series of images across the MEM−LEEM transition and we plot in Figure 5d the reflectivity spectra extracted from each domain. As with the photoemission threshold in PEEM, the shift in the MEM−LEEM transition increases with increasing poling voltage; see Table 1. The potential differences between P$^+$ and P$^-$ are reported in Table 1 for the KFM, PEEM, and LEEM experiments. For each poling voltage, the differences are similar, showing the consistency of these techniques for the surface potential measurement, although the values found in KFM are slightly lower. This might be explained by the fact that the KFM measurements were performed under nitrogen atmosphere, whereas PEEM and LEEM were operated in ultrahigh vacuum, leading to an attenuation of the potential difference. Alternatively, the absolute value of the surface potential, as measured by KFM, also depends on the tip−surface distance.

A pixel-by-pixel fit of the reflectivity curves by a complementary error function[29] allows building the MEM−LEEM transition map shown in Figure 5e. Importantly, the surface potential of P$^+$ is greater than that of P$^-$; therefore, the

Table 1. Room-Temperature Surface Potential Difference between P$^+$ and P$^-$ Poled Domains as a Function of the Applied Bias Measured by KFM, PEEM, and LEEM[a]

	bias			
	±4 V	±8 V	±10 V	±12 V
KFM	0.05	0.20		0.30
PEEM	0.24	0.33		0.49
LEEM	0.19	0.27	0.30[b]	

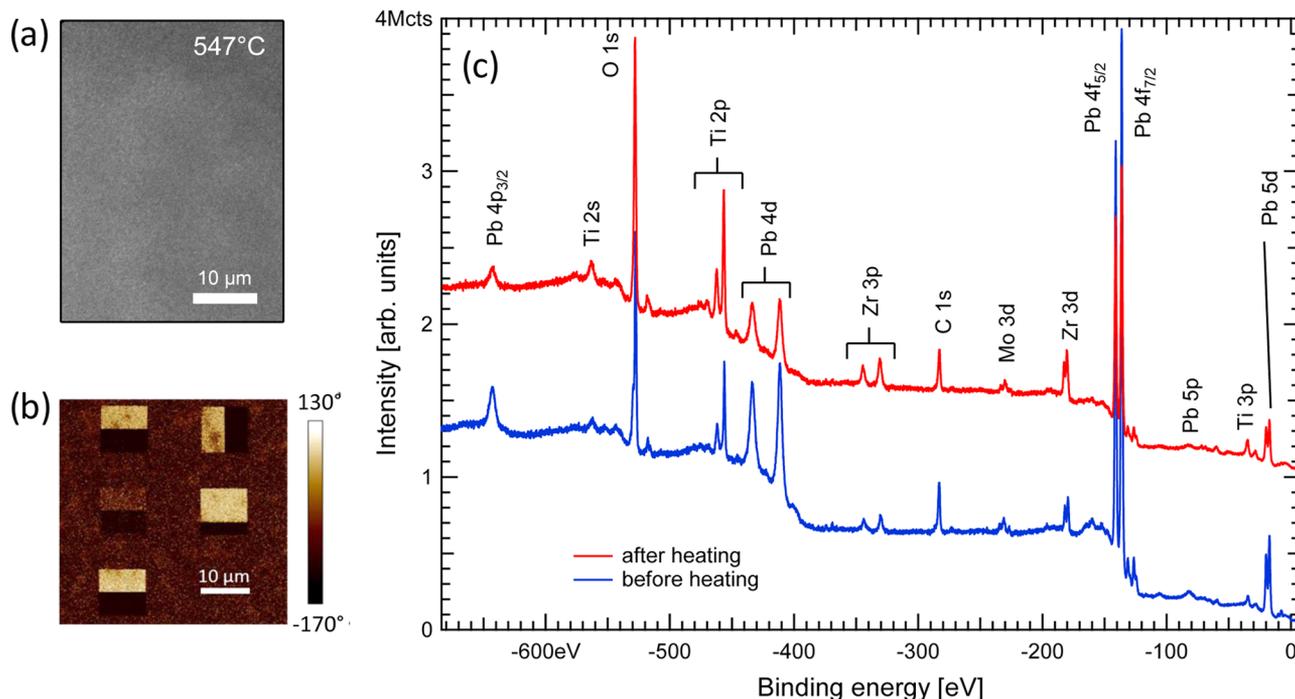[a]All values in V. [b]FE domains observed by LEEM were poled at ±10 V.

Figure 4. (a) PEEM image at $E - E_F = 4.9$ eV recorded after annealing at 547 °C. (b) PFM phase image of rewritten domains on the annealed sample. (c) XPS spectra measured at room temperature using Al Kα (1486.7 eV) photon energy for the PZT thin film before heating (blue curve) and after heating up the sample to 547 ° (red curve). Mo 3d peak corresponds to the signature of the sample holder.
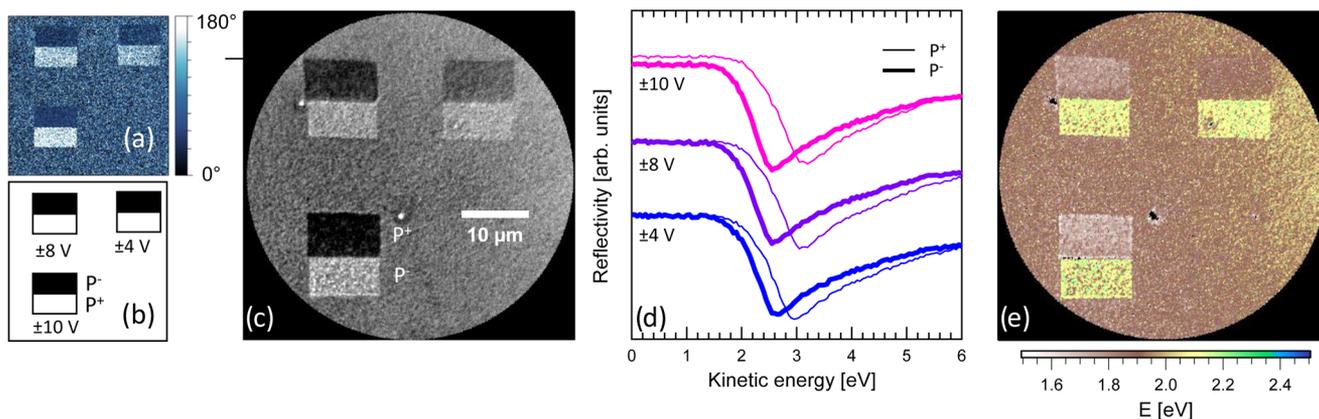

Figure 5. (a) PFM phase image of the AFM-written P$^+$ and P$^-$ domains. (b) Schematic of the written domains with different DC voltage amplitudes; white and black domains are written using negative and positive DC voltage, respectively. Each domain is 5×10 μm^2. (c) LEEM image recorded at room temperature for $E_{inc} = 2.30$ eV. (d) Reflectivity spectra extracted from the P$^+$ and P$^-$ domains written with different DC voltage amplitudes. (e) Surface potential map obtained from E_{inc} image series recorded at 22°.

sign of the domain-related potential difference is opposite to what is expected from the unscreened FE polarization orientation shown in Figure 1. We now show that this is due to screening by polar adsorbates which inverse the surface potential as seen by incident electrons.

We present the temperature dependence of the MEM–LEEM transition energy ΔE between P$^+$ and P$^-$ domains in Figure 6a, respectively. ΔE decreases as the temperature increases and crosses zero around 100 °C. Schematically, this corresponds to a situation where half of the total surface charge is perfectly screened by a polar radical, for example, HO$^-$ on P$^+$. It reaches a maximum negative value around 200 °C and then tends to zero near 500 °C.

ΔE is proportional to the difference in surface charge between P$^+$ and P$^-$ domains.[29] Above T_C, the spontaneous polarization disappears, as seen by the absence of contrast in LEEM (see Figure 6b) and PEEM images (see Figure 4a) and by the fact that ΔE tends to ≈ 0 in the range 420–450 °C in Figure 5a. This is in fair agreement with $T_C = 430$ °C for PZT and shows that the sol−gel films have FE stability similar to that of the bulk compound.[13,31]

However, the surface potential difference measured in LEEM changes sign above 100 °C, corresponding to a change in sign of the surface charge. As mentioned above, the P$^+$ domain has a higher surface potential at room temperature than the P$^-$ domain, implying negative surface charge. Thus, the change in sign can only be explained if the polarization charge is well screened by polar adsorbates, as in the left hand schematic of Figure 1. If the adsorbate species is physisorbed, for example, molecular water; then, above 100 °C it should start to desorb.
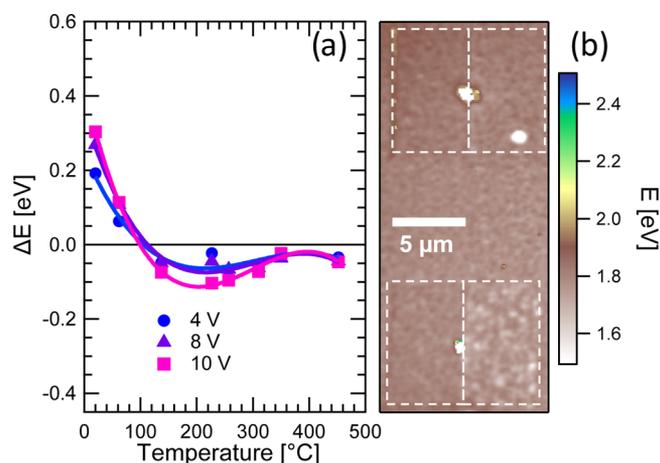
Figure 6. (a) ΔE as a function of the in situ temperature for the domains written with different DC voltage amplitudes. Lines are guidance for the eyes. (b) Surface potential map obtained from the E_{inc} image series (recorded at 452 °C) of the domains using ±4 V (top) and ±8 V (bottom) DC voltage. Domain boundaries are delimited by white dashed lines.

As a result, the surface charge, as seen by the incoming electrons, changes sign. We have quantified this desorption-induced surface potential contrast inversion between 62 and 137 °C in Figure 7. We present the reflectivity spectra in Figure
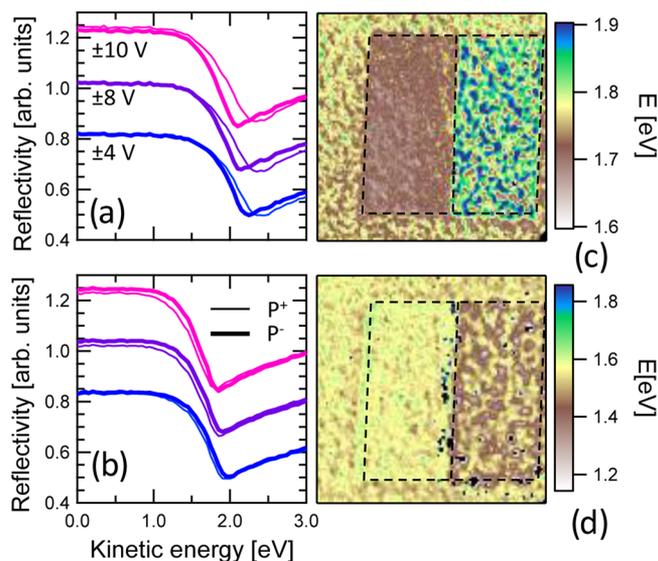

Figure 7. Reflectivity spectra extracted from the P$^+$ and P$^-$ domains written with different DC voltage amplitudes (a) and (b) data recorded at 62 and 137 °C, respectively. (c, d) Corresponding surface potential map obtained from E_{inc} image series of the domains using ±10 V DC voltage. Domain boundaries are delimited by black dashed lines.

7a, extracted from an LEEM image series acquired at 62 °C, whose MEM–LEEM transition energy map is shown in Figure 7c. The contrast between the P$^+$ and P$^-$ domains is similar to the one observed at room temperature (Figure 5d,e). On the contrary, for the measurement performed at 137 °C (Figure 7b,d), we observe that the energy of the MEM–LEEM transition in Figure 7b is lower for the P$^+$ domains than for the P$^-$ domains, meaning that the electric potential landscape has changed above the surface of each domain between the two

temperatures. This is confirmed by the reconstructed MEM–LEEM transition energy map in Figure 7d. Both the sign of the domain-related potential below 100 °C and temperature-induced surface potential inversion above 100 °C demonstrate that the polarization-bound charges are well screened by polar adsorbates, such as H_2O, below 100 °C.

4. CONCLUSIONS

In summary, we have measured FE domains written on high-quality, sol–gel grown PZT thin film by AFM using PEEM and LEEM. We observed that a clear surface potential difference exists between P$^+$ and P$^-$ domains. Furthermore, in situ temperature-dependent LEEM measurements allowed to determine the Curie temperature of PZT to be close to the bulk value of ~430 °C and the temperature-dependent desorption of polar screening charges. The experiments demonstrate that full-field electron microscopy is an excellent noncontact method for the study of the surface properties, charge state, and polarization of FE thin-film systems.

■ AUTHOR INFORMATION

Corresponding Author

*E-mail: nick.barrett@cea.fr.

ORCID

Nicholas Barrett: 0000-0002-8228-0805

Notes

The authors declare no competing financial interest.

■ REFERENCES

(1) Junquera, J.; Ghosez, P. Critical Thickness for Ferroelectricity in Perovskite Ultrathin Films. *Nature* **2003**, *422*, 506–509.

(2) Kalinin, S. V.; Bonnell, D. A.; Alvarez, T.; Lei, X.; Hu, Z.; Ferris, J. H.; Zhang, Q.; Dunn, S. Atomic Polarization and Local Reactivity on Ferroelectric Surfaces: A New Route toward Complex Nanostructures. *Nano Lett.* **2002**, *2*, 589–593.

(3) Cui, Y.; Briscoe, J.; Dunn, S. Effect of Ferroelectricity on Solar-Light-Driven Photocatalytic Activity of BaTiO3 - Influence on the Carrier Separation and Stern Layer Formation. *Chem. Mater.* **2013**, *25*, 4215–4223.

(4) Yun, Y.; Kampschulte, L.; Li, M.; Liao, D.; Altman, E. I. Effect of Ferroelectric Poling on the Adsorption of 2-Propanol on LiNbO3(0001). *J. Phys. Chem. C* **2007**, *111*, 13951–13956.

(5) Li, D.; Zhao, M. H.; Garra, J.; Kolpak, A. M.; Rappe, A. M.; Bonnell, D. A.; Vohs, J. M. Direct in situ Determination of the Polarization Dependence of Physisorption on Ferroelectric Surfaces. *Nat. Mater.* **2008**, *7*, 473–477.

(6) Wang, J. L.; Gaillard, F.; Pancotti, A.; Gautier, B.; Niu, G.; Vilquin, B.; Pillard, V.; Rodrigues, G. L. M. P.; Barrett, N. Chemistry and Atomic Distortion at the Surface of an Epitaxial BaTiO3 Thin Film after Dissociative Adsorption of Water. *J. Phys. Chem. C* **2012**, *116*, 21802–21809.

(7) Fong, D. D.; Kolpak, A. M.; Eastman, J. A.; Streiffer, S. K.; Fuoss, P. H.; Stephenson, G. B.; Thompson, C.; Kim, D. M.; Choi, K. J.; Grinberg, I.; Rappe, A. M.; et al. Stabilization of Monodomain Polarization in Ultrathin PbTiO3 Films. *Phys. Rev. Lett.* **2006**, *96*, No. 127601.

(8) Kalinin, S.; Bonnell, D. Local Potential and Polarization Screening on Ferroelectric Surfaces. *Phys. Rev. B* **2001**, *63*, No. 125411.

(9) Liu, X.; Kitamura, K.; Terabe, K. Surface Potential Imaging of Nanoscale LiNbO3 Domains investigated by Electrostatic Force Microscopy. *Appl. Phys. Lett.* **2006**, *89*, No. 132905.

(10) He, D. Y.; Qiao, L. J.; Volinsky, A. A.; Bai, Y.; Guo, L. Q. Electric Field and Surface Charge Effects on Ferroelectric Domain Dynamics in BaTiO3 Single Crystal. *Phys. Rev. B* **2011**, *84*, No. 024101.

(11) Kursumovic, A.; Defay, E.; Lee, O. J.; Tsai, C. F.; Bi, Z.; Wang, H.; MacManus-Driscoll, J. L. A New Material for High-Temperature Lead-free Actuators. *Adv. Funct. Mater.* **2013**, *23*, 5881−5886.

(12) Calame, F.; Muralt, P. Growth and Properties of Gradient Free Sol-Gel Lead Zirconate Titanate Thin Films. *Appl. Phys. Lett.* **2007**, *90*, No. 062907.

(13) Zhang, N.; Yokota, H.; Glazer, A. M.; Ren, Z.; Keen, D. A.; Keeble, D. S.; Thomas, P. A.; et al. The Missing Boundary in the Phase Diagram of PbZr1-xTixO3. *Nat. Commun.* **2014**, *5*, No. 5231.

(14) Du, X.-H.; Zheng, J.; Belegundu, U.; Uchino, K. Crystal Orientation Dependence of Piezoelectric Properties of Lead Zirconate Titanate near the Morphotropic Phase Boundary. *Appl. Phys. Lett.* **1998**, *72*, 2421−2423.

(15) Trolier-Mckinstry, S.; Muralt, P. Thin Film Piezoelectrics for MEMS. *J. Electroceram.* **2004**, *12*, 7−17.

(16) Schlom, D. G.; Chen, L.; Pan, X.; Schmehl, A.; Zurbuchen, M. A. Thin Film Approach to Engineering Functionality into Oxides. *J. Am. Ceram. Soc.* **2008**, *91*, 2429−2454.

(17) Gariglio, S.; Stucki, N.; Triscone, J.; Triscone, G. Strain Relaxation and Critical Temperature in Epitaxial Ferroelectric Pb(Zr0.20Ti0.80)O3 Thin Films. *Appl. Phys. Lett.* **2007**, *90*, No. 202905.

(18) Foster, C. M.; Bai, G.; Csencsits, R.; Vetrone, J.; Jammy, R.; Wills, L. A.; Carr, E.; Amano, J. Single-Crystal Pb (ZrxTi1-x) O3 Thin Films prepared by Metal-Organic Chemical Vapor Deposition: Systematic Compositional Variation of Electronic and Optical Properties. *J. Appl. Phys.* **1997**, *81*, 2349−2357.

(19) Kovacova, V.; Vaxelaire, N.; Rhun, G. L.; Gergaud, P.; Defay, E.; et al. Correlation between Electric-Field-induced Phase Transition and Piezoelectricity in Lead Zirconate Titanate Films. *Phys. Rev. B* **2014**, *90*, No. 140101.

(20) Gueye, I.; Le Rhun, G.; Gergaud, P.; Renault, O.; Defay, E.; Barrett, N. Chemistry of Surface Nanostructures in Lead Precursor-rich PbZr0.52Ti0.48O3 Sol-gel Films. *Appl. Surf. Sci.* **2016**, *363*, 21−28.

(21) Snitka, V.; Ulcinas, A.; Nemciauskas, K.; Lendraitis, V. AFM based Polarization Nanolithography on PZT Sol-Gel Films. *Microelectron. Eng.* **2006**, *83*, 1456−1459.

(22) Yin, S.; Niu, G.; Vilquin, B.; Gautier, B.; Le Rhun, G.; Defay, E.; Robach, Y. Epitaxial Growth and Electrical Measurement of Single Crystalline Pb(Zr0.52Ti0.48)O3 Thin Film on Si(001) for Micro-Electromechanical Systems. *Thin Solid Films* **2012**, *520*, 4572−4575.

(23) Brugère, A.; Gidon, S.; Gautier, B. Finite Element Method Simulation of the Domain Growth Kinetics in Single-Crystal LiTaO3: Role of Surface Conductivity. *J. Appl. Phys.* **2011**, *110*, No. 052016.

(24) Le Bihan, R. Study of Ferroelectric and Ferroelastic Domain Structures by Scanning Electron Microscopy. *Ferroelectrics* **1989**, *97*, 19−46.

(25) Ihlefeld, J. F.; Michael, J. R.; McKenzie, B. B.; Scrymgeour, D. A.; Maria, J. P.; Paisley, E. A.; Kitahara, A. R. Domain Imaging in Ferroelectric Thin Films via Channeling-Contrast Backscattered Electron Microscopy. *J. Mater. Sci.* **2017**, *52*, 1071−1081.

(26) Barrett, N.; Rault, J. E.; Wang, J. L.; Mathieu, C.; Locatelli, A.; Mentes, T. O.; Niño, M. A.; Fusil, S.; Bibes, M.; Barthélémy, A.; Sando, D.; Ren, W.; Prosandeev, S.; Bellaiche, L.; Vilquin, B.; Petraru, A.; Krug, I. P.; Schneider, C. M. Full Field Electron Spectromicroscopy Applied to Ferroelectric Materials. *J. Appl. Phys.* **2013**, *113*, No. 187217.

(27) Rault, J. E.; Dionot, J.; Mathieu, C.; Feyer, V.; Schneider, C. M.; Geneste, G.; Barrett, N. Polarization Sensitive Surface Band Structure of Doped BaTiO3(001). *Phys. Rev. Lett.* **2013**, *111*, No. 127602.

(28) Polisetty, S.; Zhou, J.; Karthik, J.; Damodaran, A. R.; Chen, D.; Scholl, A.; Martin, L. W.; Holcomb, M. X-ray Linear Dichroism Dependence on Ferroelectric Polarization. *J. Phys.: Condens. Matter* **2012**, *24*, No. 245902.

(29) Rault, J. E.; Ren, W.; Prosandeev, S.; Lisenkov, S.; Sando, D.; Fusil, S.; Bibes, M.; Barthélémy, A.; Bellaiche, L.; Barrett, N. Thickness-Dependent Polarization of Strained BiFeO3 Films with Constant Tetragonality. *Phys. Rev. Lett.* **2012**, *109*, No. 267601.

(30) Wang, J. L.; Vilquin, B.; Barrett, N. Screening of Ferroelectric Domains on BaTiO3(001) Surface by Ultraviolet Photo-induced Charge and Dissociative Water Adsorption. *Appl. Phys. Lett.* **2012**, *101*, No. 092902.

(31) Jaffe, B.; Cook, W. R.; Jaffe, H. L. *Piezoelectric Ceramics*; Non-Metallic Solids; Elsevier Science: London, 2012.